

Origin of the anomalously rocky appearance of Tsiolkovskiy crater



Benjamin T. Greenhagen^{a,*}, Catherine D. Neish^b, Jean-Pierre Williams^c, Joshua T.S. Cahill^a, Rebecca R. Ghent^{d,e}, Paul O. Hayne^f, Samuel J. Lawrence^g, Noah E. Petro^h, Joshua L. Bandfieldⁱ

^a Johns Hopkins University Applied Physics Laboratory, 11100 Johns Hopkins Road, Laurel, MD 20723-6099, United States

^b Department of Earth Sciences, Western University Biological & Geological Sciences Building, Room 1026 1151 Richmond St. N. London, ON N6A 5B7 Canada

^c Department of Earth, Planetary, and Space Sciences, University of California, Los Angeles 595 Charles Young Drive East, Box 951567 Los Angeles, CA 90095-1567, United States

^d Department of Earth Sciences, Earth Sciences Centre 22 Russell Street Toronto, Ontario, M5S 3B1, Canada

^e Planetary Science Institute, 1700 East Fort Lowell, Suite 106 Tucson, AZ 85719-2395, United States

^f Jet Propulsion Laboratory, California Institute of Technology, 4800 Oak Grove Drive Pasadena, CA 91109 ASU, United States

^g School of Earth and Space Exploration, PO Box 871404 Tempe, AZ 85287-1404, United States

^h NASA's Goddard Space Flight Center, 8800 Greenbelt Rd Greenbelt, MD 20771, United States

ⁱ Space Science Institute, 4750 Walnut Street | Suite 205 Boulder, Colorado 80301, United States

ARTICLE INFO

Article history:

Received 3 August 2015

Revised 6 February 2016

Accepted 22 February 2016

Available online 10 March 2016

Keywords:

Moon, surface

Cratering

Impact processes

Geological processes

Regoliths

ABSTRACT

Rock abundance maps derived from the Diviner Lunar Radiometer instrument on the Lunar Reconnaissance Orbiter (LRO) show Tsiolkovskiy crater to have high surface rock abundance and relatively low regolith thickness. The location of the enhanced rock abundance to the southeast of the crater is consistent with a massive, well-preserved impact melt deposit apparent in LRO Miniature Radio Frequency instrument circular polarization ratio data. A new model crater age using LRO Lunar Reconnaissance Orbiter Camera imagery suggests that while it originated in the Late Imbrian, Tsiolkovskiy may be the youngest lunar crater of its size (~180 km diameter). Together these data show that Tsiolkovskiy has a unique surface rock population and regolith properties for a crater of its size and age. Explanation of these observations requires mechanisms that produce more large blocks, preserve boulders and large blocks from degradation to regolith, and/or uncover buried rocks. These processes have important implications for formation of regolith on the Moon.

© 2016 Elsevier Inc. All rights reserved.

1. Introduction

The approximately 180 km diameter lunar farside crater Tsiolkovskiy (20.4°S, 129.1°E; Figs. 1 and 2) is partially filled by mare basalt has a well preserved central peak, and is associated with distinct impact melt and ejecta deposits (Guest and Murray, 1969; Guest, 1971; Wilhelms and El-Baz, 1977; Whitford-Stark and Hawke, 1982; Pieters and Tompkins, 1999). Since it was first imaged, Tsiolkovskiy crater has been recognized as an enigmatic feature on the lunar surface. Reviewing its first identification from Luna 3 photography, Barabashov (1962) wrote: “This crater has been termed the ‘Tsiolkovskiy Crater’. It merits special attention for it has a particularly dark bottom and an exclusively bright central hill: the brightness of the central hill is quite great, and one is led to wonder whether or not it might be self-luminescent”.

Its mare-filled floor stands in stark contrast to the central peak and surrounding highlands and is one of the few exposures of mare basalt on the lunar farside. Therefore Tsiolkovskiy provides a valuable reference point for evaluating lunar farside mare production specifically and the history of lunar volcanism generally. However, while the composition of Tsiolkovskiy’s geologic units has been substantially constrained using a range of remote sensing datasets (e.g., Pieters and Tompkins, 1999; Matsunaga et al., 2008; Cheek and Pieters, 2012); the geologic history and evolution of the crater remain uncertain, especially considering the regional setting of Tsiolkovskiy, which is otherwise typical lunar highlands.

Recently, data from the Lunar Reconnaissance Orbiter (LRO) have been used to identify a thermophysical anomaly at this enigmatic crater (Greenhagen et al., 2013). The Diviner Lunar Radiometer (Diviner) on the LRO has observed Tsiolkovskiy to have unusually high surface rock abundance for a crater of its reported age, >3.2 Ga based on a variety of cumulative crater frequency studies of the mare fill (Tyrie, 1988; Williams et al., 2013; Pasckert et al., 2015). Most regions of high rock abundance on

* Corresponding author. Tel.: +1 240 228 1499; fax: +1 240 228 8939.

E-mail address: benjamin.greenhagen@jhuapl.edu (B.T. Greenhagen).

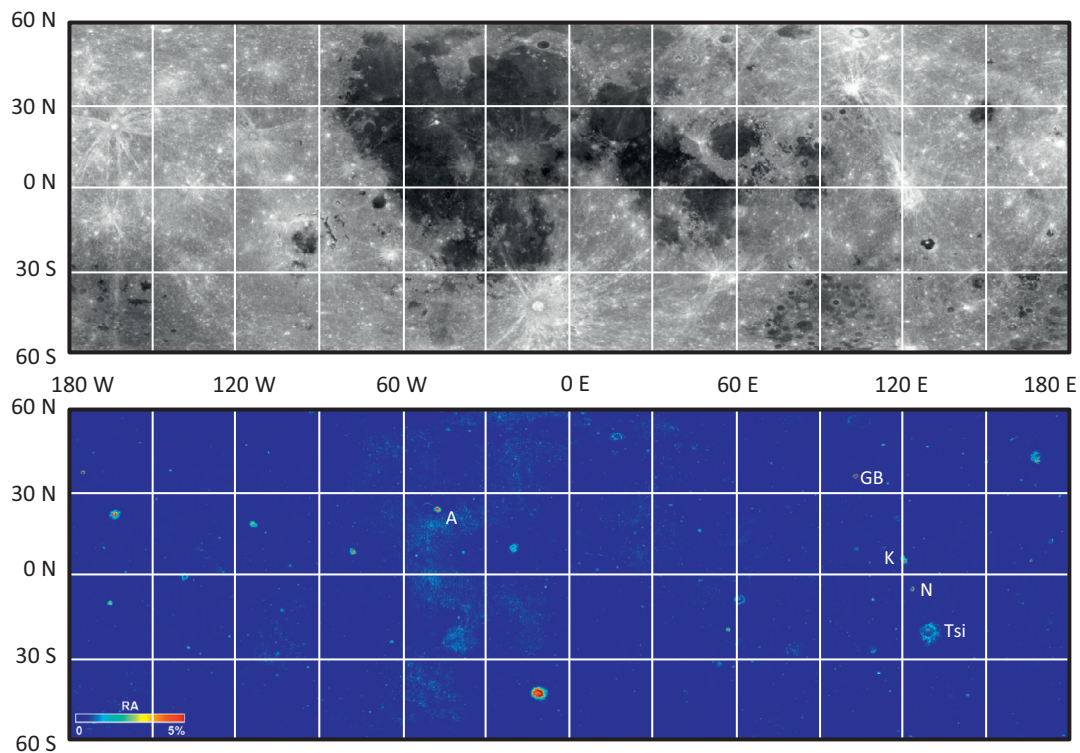


Fig. 1. Even at global scales Tsiolkovskiy crater (Tsi) has a relatively fresh appearance (top - LROC WAC normalized albedo) and its rock abundance anomaly is readily apparent (bottom - Diviner rock abundance). Tsiolkovskiy is nearly antipodal to Aristarchus crater (A) and is located along a bright ray intersecting Giordano Bruno (GB), King (K), and Necho (N) craters.

the Moon are associated with boulder-rich ejecta blankets around Copernican-aged craters (Bandfield et al., 2011; Ghent et al., 2014; Fig. 1). The location of this rock abundance anomaly, to the south-east of the crater (Fig. 2), is generally coincident with an impact melt deposit first identified in images by Hawke and Head (1977) and more recently characterized by Neish et al. (2014) using Mini-RF data. In this study, we further describe the nature and relationship between the rock abundance anomaly and the crater's impact melt and ejecta. We update estimates for Tsiolkovskiy's age using new images from LRO and discuss potential formation mechanisms for the observed rock abundance anomaly.

2. Methods and datasets

This study primarily uses LRO datasets from Diviner, the Miniature Radio Frequency instrument (Mini-RF), and the Lunar Reconnaissance Orbiter Camera (LROC). Data from Diviner are used to map the surficial distribution of meter-scale rocks and cohesive, high thermal inertia materials as well as the approximate thickness of the non-rocky regolith component. Mini-RF data are used to characterize the decimeter-scale roughness on the surface and in the near-subsurface, which are helpful for mapping the extent of the impact melt deposit. LROC Wide Angle Camera (WAC) mosaics are used for a new crater count study to model the age of Tsiolkovskiy and LROC Narrow Angle Camera (NAC) imagery are used for inspection of the geologic relationships at scales of 1–2 m.

Diviner has nine spectral channels that span the visible, near-infrared, and thermal infrared wavelengths (Paige et al., 2010). Diviner's rock abundance estimates leverage the wavelength dependence of thermal emission for scenes of mixed temperatures. Bandfield et al. (2011) produced a model for simultaneously solving for the areal fraction of rocks greater than ~0.5 to 1 m in diameter and the temperature of the rock-free regolith using

thermal models and nighttime data from three of Diviner's broad thermal channels: Ch. 6 (13–23 μm), Ch. 7 (26–41 μm), and Ch. 8 (50–100 μm). Global 128 pixels per degree maps of Diviner rock abundance and rock-free regolith temperature are archived in the NASA Planetary Data System Geoscience Node. Hayne et al. (this issue) have used the Diviner rock-free regolith temperature data to calculate an approximate scale height (H) of the uppermost insulating regolith layer. This " H -parameter" is inversely correlated to bulk thermal inertia (Hayne et al., this issue). We use both the Diviner rock abundance and H -parameter products to characterize the variations in thermophysical properties around Tsiolkovskiy crater.

Ghent et al. (2014) used the Diviner rock abundance dataset to investigate characteristic values for crater ejecta as a function of crater model ages and derive an empirical constraint on the breakdown rate of rocky ejecta materials, which provided a new method for dating young lunar impact craters. At the heart of this work was recognition that rock abundances for rocky features such as impact craters do not follow normal or lognormal distributions (while the nearly rock-free background does; Fig. 3); therefore, statistical parameters used to represent the central tendency are not adequate to capture the variation of rock abundance values. Instead, Ghent et al. (2014) introduced the $RA_{95/5}$ parameter, which is the threshold value separating the highest 5% of a given crater's ejecta rock abundance values from the lower 95%. $RA_{95/5}$ is strongly correlated with modeled crater age (Ghent et al., 2014). A key assumption of this technique is that ejected rocky materials are emplaced at the time of impact, and are subsequently eroded and/or buried by the effects of micrometeoroids and small bolides. In calculating their regression, Ghent et al. (2014) avoided terrain interior to crater rims, which due to the presence of steep slopes, can experience mass wasting that replenishes the surface rock population, and large melt deposits, which represent a ready

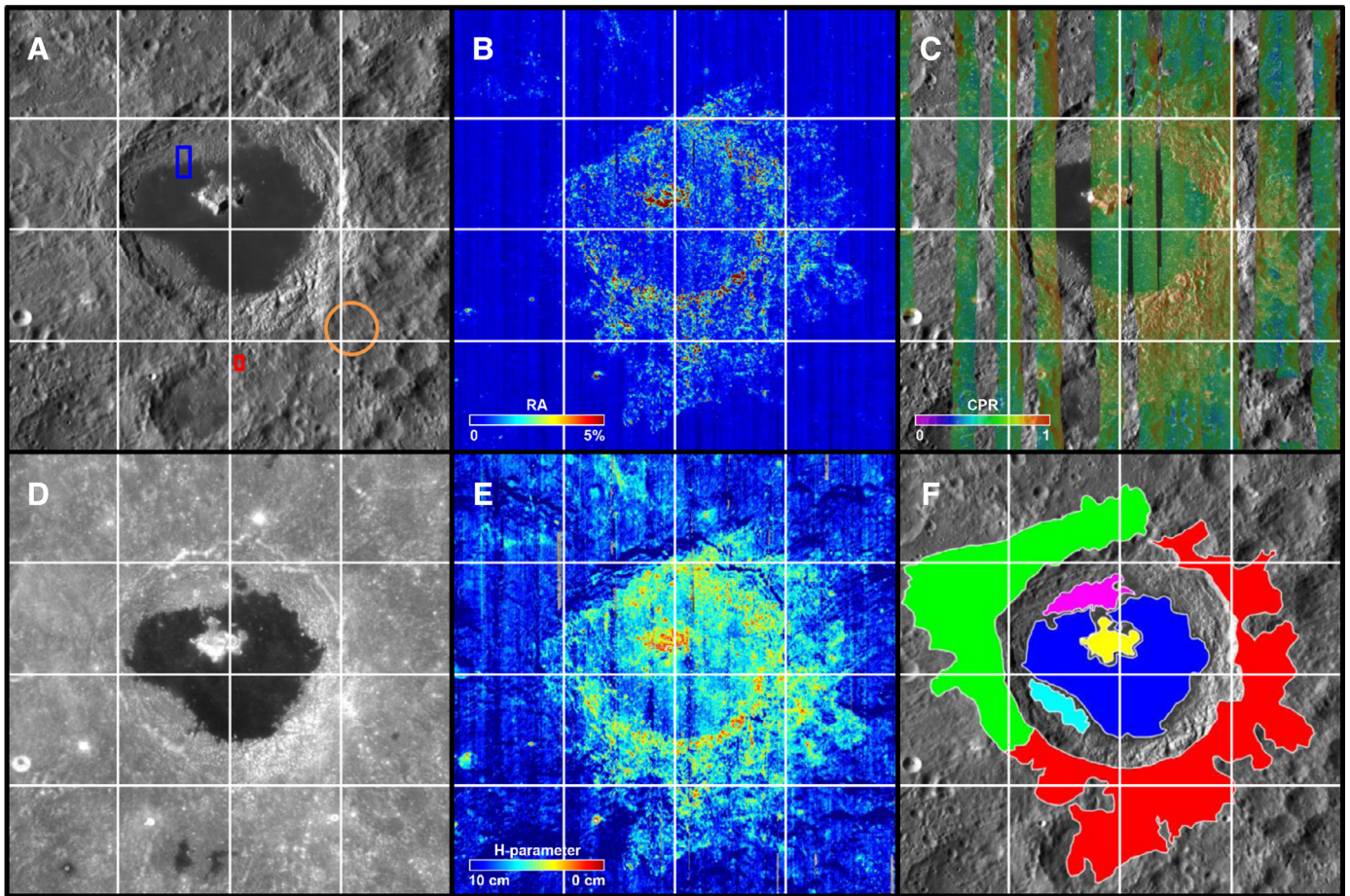


Fig. 2. Tsiolkovskiy crater as seen in various datasets from LRO (bounds are 27°S to 15°S; 123°E to 135°E): (A) LROC WAC morphological mosaic, (B) Diviner rock abundance, (C) Mini-RF CPR, (D) LROC WAC 689 nm normalized albedo, (E) Diviner *H*-parameter, and (F) ROIs used in the rock abundance study. The ROIs are central peak (yellow), mare-fill crater floor (blue), non-mare crater floor (purple/cyan), Diviner rock abundance anomaly (red), and non-rocky ejecta (green). The antipode of Aristarchus, discussed in Section 4.3, is indicated by the orange circle in (A). The approximate positions of Figs. 5A and 6A are also indicated in by the blue and red boxes respectively in (A). The Diviner rock abundance anomaly is correlated with relatively high values in Mini-RF CPR and relatively low values in Diviner *H*-parameter. (For interpretation of the references to color in this figure legend, the reader is referred to the web version of this article.)

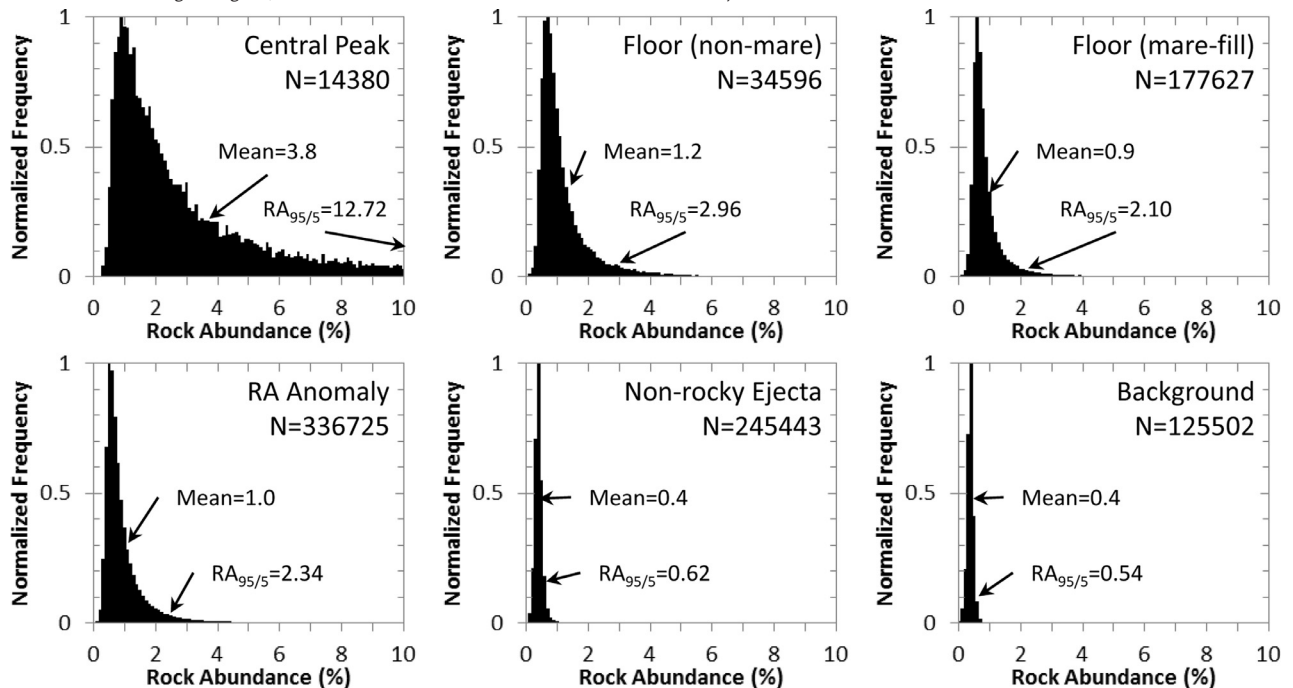


Fig. 3. Histograms of rock abundance (RA) values for ROIs around Tsiolkovskiy crater; mean RA, and $RA_{95/5}$ (95th percentile RA value) are indicated. *N* is the number of 128 pixels per degree bins included in the statistical sample. Additional statistics are provided in Table 1.

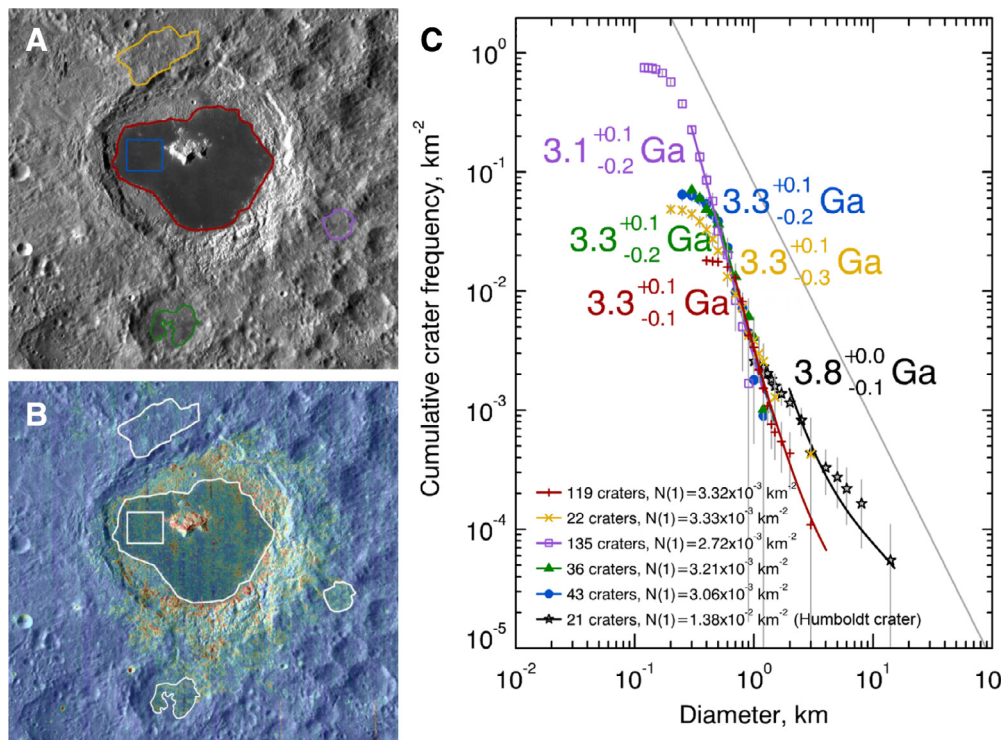


Fig. 4. Impact crater size-frequency distributions and absolute model ages of crater counts were calculated for areas shown in (A) LROC WAC morphological mosaic and (B) Diviner RA overlay on LROC WAC are provided in (C) plotted with Craterstats2 (Michael and Neukum, 2010) using the Neukum et al. (2001) production function. Areas in and around Tsiolkovskiy are interior mare deposits ($D > 500$ m; red outline/trace), subset of interior mare deposit ($D > 200$ m; blue outline/trace), non-rocky primary ejecta ($D > 200$ m; yellow outline/trace), melt deposits exterior to the crater ($D > 200$ m; green and purple outlines/traces). Williams et al. (2013) crater counts from the floor of Humboldt crater ($D > 1$ km; black trace) are also provided. (For interpretation of the references to color in this figure legend, the reader is referred to the web version of this article.)

source of new surface rocks associated with the formation of small craters into them. Both these effects would lead to an erroneously young age if the Ghent et al. (2014) chronology were applied blindly. With these caveats in mind, we investigate the relative variation in $RA_{95/5}$ for different areas in and around Tsiolkovskiy, and interpret the implications for its chronology.

Mini-RF is a hybrid dual-polarized Synthetic Aperture Radar with two wavelengths (S-Band, 12.6 cm, and X-Band, 4.2 cm) and two resolutions (150 m and 15 m) (Nozette et al., 2010). Cahill et al. (2014) produced a circular polarization ratio (CPR) data product based on the Mini-RF S-Band 100 m/pixel global mosaic. CPR is defined as the ratio of the backscattered power in the same polarization that was transmitted to the opposite-sense circular polarization. Smooth surfaces are dominated by single-bounce reflections and have low CPR, while rough surfaces are dominated by multiple-bounce reflections and tend to have relatively high CPR. As recently demonstrated by Neish et al. (2014), CPR is an effective tool for surveying impact melts because they tend to be very rough at radar wavelengths. We use the Mini-RF CPR mosaic to identify surface and near-surface impact melt deposits around Tsiolkovskiy crater.

The LROC WAC is a 7-color push-frame camera with 100–400 m spatial sampling (Robinson et al., 2010). We use monochromatic WAC imagery with a sampling of 100 m/pixel to count craters larger than ~ 500 m across Tsiolkovskiy's entire mare-filled floor and larger than ~ 200 m for a smaller areas in and around the crater (Fig. 4), avoiding clusters of obvious secondary craters and volcanic craters. After compiling statistics, we use the Neukum et al. (2001) chronology to model the age of the mare-fill. Additionally, we use LROC NAC monochromatic imagery with a resolution ~ 1 m/pixel to investigate the relationships between surface features and the morphology of the rock populations, which are readily apparent in the images.

Due to the considerable ambiguity in the literature regarding size terminology for rocky materials (i.e. cohesive materials with high thermal inertia), we define the following terms used in this paper: small blocks are <0.25 m, boulders are 0.25–10 m, large blocks are 10–1000 m, and megablocks are >1000 m. In terms of the datasets analyzed, Diviner and LROC are capable of observing boulders and large blocks exposed on the surface, while Mini-RF is sensitive to small blocks and some boulders on the surface or in the near-subsurface.

3. Observations

Tsiolkovskiy crater has a remarkably high rock abundance for an impact crater of its reported age (>3.2 Ga; Tyrrie, 1988; Williams et al., 2013; Pasckert et al., 2015) based upon crater size frequency distributions. Here we examine different regions of interest (ROIs) in and around Tsiolkovskiy crater to investigate what clues they provide us about the crater's age and subsequent modification (Fig. 2F; Table 1).

3.1. Central peak

Rising over 3 km above the crater floor, the central peak and rim have steep slopes and ongoing mass-wasting induced surface rock formation. Therefore, these regions represent the typical roughness and rock-rich geomorphology of a nearly continuously replenished unit, an important endmember for investigating the rock abundance of the region. The unit with Tsiolkovskiy's highest rock abundance is the central peak with an ROI-averaged $RA_{95/5}$ of 12.72% (Table 1). This value is slightly higher than the $RA_{95/5}$ of the ejecta blanket of Giordano Bruno ($RA_{95/5} = 12.44\%$; Ghent et al., 2014), which is expected given that the rocky Giordano Bruno materials have not been replenished since crater formation

Table 1

Rock abundance and *H*-parameter statistics are included for the ROIs around Tsiolkovskiy crater shown in Fig. 2F. Samples is the number of 128 pixels per degree bins included in the statistical sample. Histograms of rock abundances are provided in Fig. 3.

Region of interest	Rock abundance (%)					<i>H</i> -parameter (cm)	
	Samples	Mean	Median	Mode	RA _{95/5}	Mean	Std. dev.
Central peak	14,380	3.8	2.2	0.9	12.72	4.0	2.1
Floor (non-mare)	34,596	1.2	0.9	0.6	2.96	6.0	1.4
Floor (mare-fill)	177,627	0.9	0.7	0.6	2.10	6.8	1.5
RA anomaly	336,725	1.0	0.7	0.5	2.34	6.9	1.6
Non-rocky ejecta	245,443	0.4	0.4	0.4	0.62	8.6	1.3
Background	125,502	0.4	0.4	0.4	0.54	9.2	1.6

(4 ± 1.2 Ma, Morota et al., 2009; 5–10 Ma, Basilevsky and Head, 2012). ROIs around Tsiolkovskiy with lower RA_{95/5} values must have a lower replenishment rate, a longer time since formation/replenishment, or both. A replenishment rate greater than zero effectively makes surfaces appear younger; therefore, we can use RA_{95/5} and the Ghent et al. (2014) chronology to establish an equivalent age of the boulder- and large block-rich terrain being exposed, which is distinct from the formation age of Tsiolkovskiy.

3.2. Crater floor

3.2.1. Crater counts

The floor of Tsiolkovskiy crater is partially filled with one of the largest continuous mare deposits on the lunar farside. The existence of this deposit is fortuitous in that it provides a flat, uniform surface on which to perform crater-counting studies. Ages derived from these counts provide a robust lower limit on the age of the crater, since the mare-fill post-dates crater formation. Gornitz (1973) used relative cumulative crater frequencies and reported a mare fill age between those of Mare Tranquillitatis and Oceanus Procarrum (3.2–3.6 Ga), and found it was not significantly younger than the crater ejecta. Walker and El-Baz (1982) used the intersection of the observed crater production and steady state curves with the age calibration from Boyce and Johnson (1977) and determined the age of the mare was 3.8 Ga. Tyrle (1988) compared the cumulative frequencies of the mare with the cumulative frequencies and radiometric ages at the Apollo 15 landing site to interpolate an age of 3.51 ± 0.1 Ga. Recently, Pasckert et al. (2015) investigated a 100 km² area of the mare deposit using crater size-frequency distribution measurements and the production and chronology functions of Neukum et al. (2001) and determined an absolute model age of $3.19 (+0.08/-0.12)$ Ga with 4 km² subdivisions providing ages between 2.22 and 3.69 Ga, the spread in ages they attribute to younger cratering and/or volcanic events. In geologic maps based on stratigraphic relationships, Tsiolkovskiy crater and its mare fill have been assigned Upper or Late Imbrian (>3.2 Ga) ages (Wilhelms and El-Baz, 1977; Wilhelms, 1987).

In this work, we provide independent cumulative crater size-frequency distributions and calculated absolute model ages, based on the Neukum et al. (2001) chronology, for Tsiolkovskiy's mare fill and non-rocky primary ejecta, and impact melt exterior to the crater (Fig. 4). On the mare deposit, several clusters of secondary craters in the eastern region and numerous volcanic craters were avoided. In all, we identified 119 craters (diameter $D > 500$ m) over an area of 9192 km² and calculate an age of $3.32 + 0.06 - 0.08$ Ga. We also compiled statistics for 43 smaller craters ($D > 200$ m) for a subset of the western mare deposit ($A = 1115$ km²) and find a similar age of $3.25 + 0.11 - 0.23$ Ga. An area of non-rocky primary ejecta north of the crater rim produces an age of $3.32 + 0.11 - 0.28$ Ga. Finally, we examined two separate areas of the rock abundance anomaly, on the eastern edge and a southern lobe that partially filled Waterman crater,

and determine absolute model ages of $3.10 + 0.11 - 0.18$ Ga and $3.30 + 0.10 - 0.21$ Ga, respectively. We find the areas outside the crater produce ages indistinguishable from the areas of mare fill and therefore the mare emplacement must have occurred soon after the crater forming impact.

3.2.2. Surface rock distribution

Additional analyses were performed on the portion of the crater floor not covered by mare deposits, presumably revealing the original crater floor. Approximately 20% of the crater floor has not been covered with mare and can provide statistics for the weathering of a massive continuous impact melt and megablock deposit. The two largest preserved areas are located in the W-NW and W-SW regions of the crater floor (Fig. 2). Together these areas have a RA_{95/5} of 2.96%, the second highest of any ROI, while the mare-filled floor has a RA_{95/5} of 2.10% (Table 1). LROC NAC imagery provides a detailed view of the floor (Fig. 5). In the mare-filled area, fresh materials are produced and exposed directly by impacts, whereby less weathered blocks and boulders can be found inside and around small craters (Fig. 5E). This process also occurs in the crater floor not covered by mare basalt (Fig. 5D); however, here two additional processes not observed in the mare also aid surface rock production. First, impacts adjacent to small hills tend to disrupt the regolith on the slopes and tops of the hills, exposing surface rocks of greater size and at greater distances from the crater (Fig. 5C). Second, there are populations of rocks not immediately associated with nearby fresh impacts and often correlated with elevated terrains (Fig. 5B). In addition to having enhanced surface rock abundances, the original crater floor also has higher CPR than the mare fill. This implies enhanced decimeter- to meter-scale roughness on the surface or in the near-subsurface (buried beneath as much as ~1 m of regolith).

3.3. Exterior crater deposits

The distribution of surface rocks outside Tsiolkovskiy is clearly asymmetric, with a strong rock abundance anomaly found in a region extending eastward from outside the southern rim to outside the northeastern rim (Fig. 2B). These surface boulders and large blocks are highly correlated with the area of enhanced CPR near Tsiolkovskiy (Fig. 2C) and the morphology of this area is consistent with previous identifications of massive impact melt deposits using Mini-RF data (Carter et al., 2012; Neish et al., 2014). Specifically, the rocky deposit southeast of Tsiolkovskiy has enhanced CPR and clearly defined lobate margins characteristic of melt flow. The origin of the asymmetric deposit is uncertain but may be due to an oblique impact (Craddock and Greeley, 1988) or pre-impact local topography and regional slopes (Hawke and Head, 1977).

We used LROC NAC images to investigate the morphology and spatial distribution of boulder and large block populations within the rock abundance anomaly and find it is largely similar to that of the original crater floor; with surface rocks directly

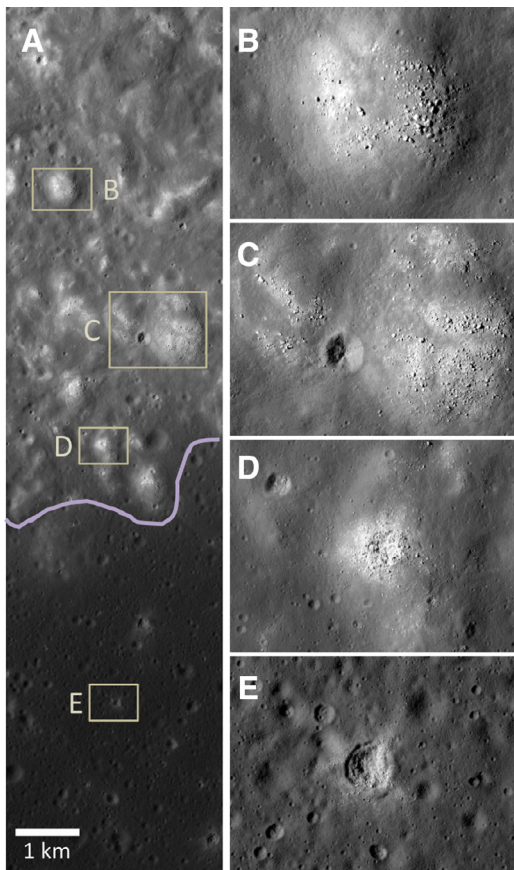


Fig. 5. LROC NAC imagery are used to investigate the spatial distribution and morphology on the crater floor of Tsiolkovskiy: (A) context view across the original floor with approximate mare-fill boundary (pale purple line), (B) an isolated population of surface rocks on elevated terrain (18.98°S/127.77°E), (C) surface rock formation adjacent to impact crater, (D) direct ejection of boulders from impact melt, (E) direct ejection of boulders from maria. The image resolution is ~ 0.9 m/pixel with 54.31° solar incidence (LROC NAC Frame: M1098016380L). (For interpretation of the references to color in this figure legend, the reader is referred to the web version of this article.)

exposed by small impacts, proximal to small impacts, and in isolated populations at elevated terrain (Fig. 6). The larger melt flow also includes numerous impact melt ponds, smooth impact melt deposits with relatively lower surface rock abundances that are similar to the mare-filled crater floor. Surface rock populations associated with the impact melt ponds outside the crater are predominantly exposed by small impacts and mass wasting along flow features (Fig. 6).

The rock abundance anomaly ROI has a $RA_{95/5}$ value of 2.34%, which is higher than mare-filled floor and suggests more efficient surface rock production than the flat, cohesive maria (Table 1). Not surprisingly, the rock abundance anomaly has a lower $RA_{95/5}$ than the original crater floor indicating a lower surface rock replenishment rate. In contrast, the area of ejecta beyond the northwestern rim, despite producing a similar absolute model age to areas in the rock abundance anomaly, is relatively devoid of surface rocks ($RA_{95/5} = 0.62\%$) and has the lowest CPR of any ROI. Using the Ghent et al. (2014) chronology to calculate an average exposure age for the rock abundance anomaly terrain gives a surprisingly young age of 204 Ma. This is much lower than crater-counting modeled ages and stratigraphy described in Section 3.2.1 and is evidence for substantial surface rock replenishment.

Diviner H-parameter scales with the thickness of the highly insulating rock-free regolith layer and eventually saturates to the local background value (~ 9.2 cm at Tsiolkovskiy). H-parameter values lower than the local background value represent areas that

are not in regolith equilibrium, indicating they are younger than ~ 1.5 Ga or they are undergoing regolith wasting or rock production (Hayne et al., this issue). The H-parameter value is 6.9 cm for the rock abundance anomaly ROI (Table 1), which is low considering the modeled age for the crater. The H-parameter for the rock abundance anomaly is significantly higher than the central peak (4 cm) and similar to the bulk crater floor (6.0 and 6.8 cm for the original and non-mare crater floors, respectively). Interestingly, the relatively rock-free ejecta, which is nearly indistinguishable from background in Diviner rock abundance and Mini-RF CPR data, has a slightly sub-background H-parameter value of 8.6 cm, or $\sim 93\%$ of the background value.

4. Discussion

4.1. Comparisons with other craters

In terms of its unusually rocky appearance, Tsiolkovskiy is unique for its size and age. Therefore, it is not possible to directly compare Tsiolkovskiy with similar craters; craters of similar size are older and clearly more degraded (e.g., Humboldt), craters of similar age are smaller (e.g., Theophilus, Langrenus) and craters with similar ejecta rock abundances are much younger and smaller, incapable of producing the large blocks and massive impact melt observed at Tsiolkovskiy. However, individual aspects of these craters are relevant, which we examine here.

Theophilus crater (11.5°S, 26.3°E; Fig. 7) is a ~ 99 km diameter crater, described as Erastothenean (1.1–3.2 Ga) in age (Wilhelms, 1987). Hawke and Head (1977) identified melt deposits to the NE of the crater, and lobate regions of high CPR have been observed north of the crater by Mini-RF (Neish et al., 2013). These observations are consistent with previous observations of melt deposits by the Mini-RF instrument, which detected ponds and flows around Erastothenean-aged craters but not around more degraded craters of Imbrian age (Carter et al., 2012; Shankar et al., 2013; Neish et al., 2014). The Diviner rock abundance of this particular melt deposit is, however, low compared to Tsiolkovskiy crater and surface rock populations are most clearly associated with small impact craters and impact melt flow scarps. This is also consistent with Ghent et al. (2014) who showed that most surface boulders identifiable in Diviner data are degraded to or covered by regolith in ~ 1 Ga. After that point, decimeter- to meter-scale blocks and boulders around Erastothenean craters can still be identified in the near subsurface (up to ~ 1 m depth) by S-Band radars such as Mini-RF (Campbell, 2002; Neish et al., 2011).

Langrenus crater (8.9°S, 61.0°E; Fig. 7) is a ~ 132 km diameter crater, described as Erastothenean in age (Wilhelms, 1987). Hawke and Head (1977) identified exterior melt deposits to the SSE of the crater. Although there is no significant enhancement in Diviner rock abundance data, impact melt ponds southeast of the crater rim do show higher than average CPR (Fig. 7). Williams et al. (2013) examined a smooth deposit in the SSE region of the crater floor and reported that Langrenus was older than Tsiolkovskiy based on relative crater size-frequency distributions. Being both older and smaller than Tsiolkovskiy could explain its more degraded state in the Diviner rock abundance dataset.

Humboldt crater (27.0°S, 81.0°E) is a ~ 200 km diameter crater, described as Late Imbrian (3.2–3.8 Ga) in age (Wilhelms, 1987). Williams et al. (2013) also reported that Humboldt is older than Tsiolkovskiy and their data are consistent with the upper end of this age range (Fig. 4). Hawke and Head (1977) identified exterior melt deposits to the SE and ENE of the crater; however, Humboldt lacks significant enhancement in radar CPR or rock abundance. Although larger than Tsiolkovskiy, the massive exterior melt deposits outside of Humboldt have eroded to the point where they are indistinguishable from the rock abundance and decimeter- to

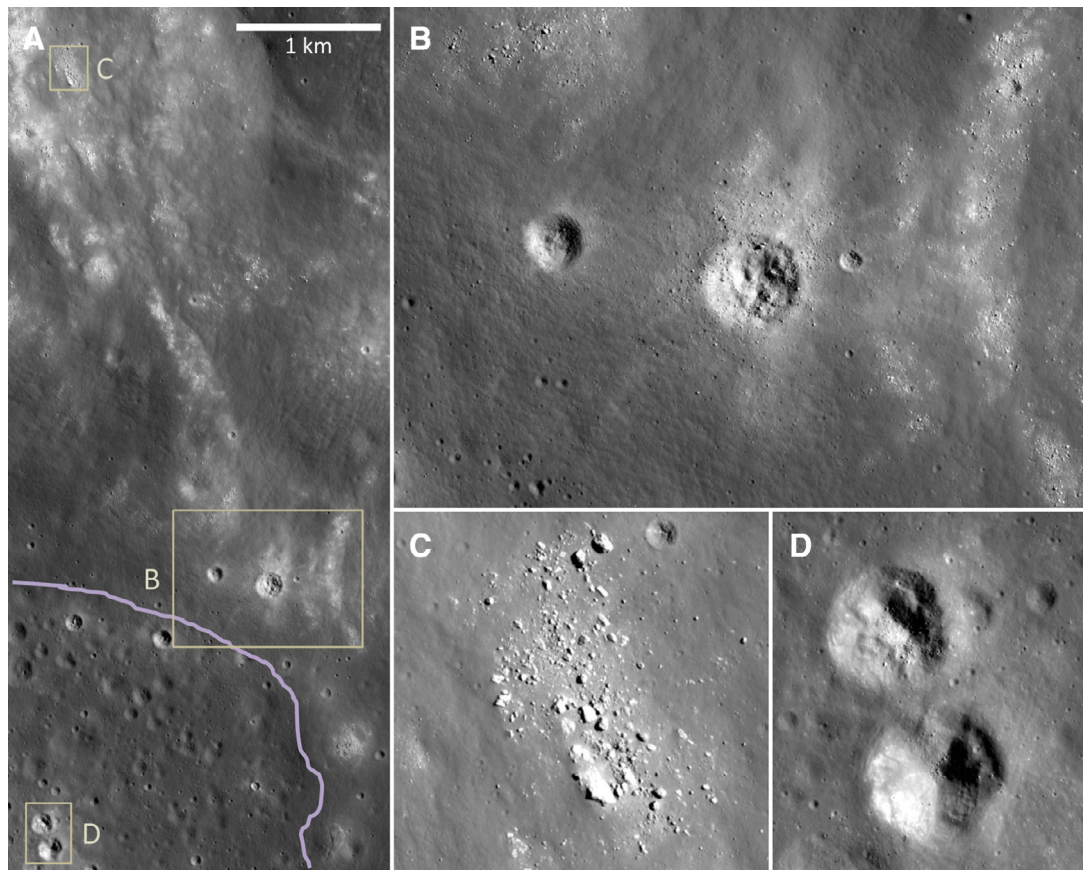


Fig. 6. The morphology and spatial distribution of rocky areas in the rock abundance anomaly share similarities with the crater floor (Fig. 5): (A) context view across a portion of the rock abundance anomaly with approximate boundary of an isolated impact melt pond (pale purple line), (B) impact crater (24.54°S/129.37°E) with boulder ejection and proximal regolith removal exposing surface rocks, (C) an isolated population of surface rocks on elevated terrain, (D) rocky impact craters in the impact melt pond. The image resolution is ~ 0.9 m/pixel with 57.67° solar incidence (LROC NAC Frame: M1168684799R). (For interpretation of the references to color in this figure legend, the reader is referred to the web version of this article.)

meter-scale surface and near-subsurface roughness of the background regolith. However, detailed examination using LROC NAC imagery of scarce surface rock populations in Humboldt's impact melt region show similar morphology to the much more abundant surface rock populations around Tsiolkovskiy. Together these observations support the hypothesis that Humboldt produced impact melt and primary ejecta rich in boulders and large blocks similar to Tsiolkovskiy but presently has a much thicker regolith cover.

4.2. Surface block production and preservation

Surface rock populations associated with degrading impact melt deposits and non-melt primary ejecta likely differ significantly. Impact melt deposits are mixtures of clasts and melted material emplaced during the late stages of impact crater formation, which cool to form solidified veneers, ponds, and flows (Howard and Wilshire, 1975). Impact melt deposits appear rough with high CPR in S-Band radar data whether or not surface rocks are present (Neish et al., 2014). However, smooth impact melt deposits typically have a few surface rocks in Diviner data (Bandfield et al., 2011). To produce surface rocks visible in Diviner data, recent impacts must be large enough to penetrate the regolith and excavate meter-scale boulders from the coherent melt deposit (Fig. 9A and B).

On the other hand, rocky materials in the non-melt primary ejecta are produced directly during impact and degrade with time (Ghent et al., 2014). Furthermore, large impact events expose and eject large blocks of coherent material that are tens to hundreds of

meters in size, and there is clear evidence for blocks this large still present within the rock abundance anomaly around Tsiolkovskiy (Fig. 8). These large blocks would weather into regolith more slowly with continuous mass wasting of cobbles and fines from the margins and catastrophic rupture until the local regolith effectively grows high enough to cover the large blocks (Fig. 9C and D). Regolith cover of ~ 1 m effectively preserves blocks and boulders of all scales in the subsurface for billions of years, causing them to be invisible to both Diviner and Mini-RF (Ghent et al., 2015), with large buried blocks reflected in the hummocky topography. These deposits only produce new surface rocks when recent impact craters of sufficient size happen to penetrate the regolith cover and hit buried rocky material. Therefore, fresh boulder-rich ejecta will have much higher rock abundance than impact melt deposits, and degraded boulder-rich ejecta will have much lower surface rock abundances. Because of its age and lack of surface rocks, the area of ejecta beyond Tsiolkovskiy's northwestern rim is consistent with this model of non-melt primary ejecta degradation for a Late Imbrian or Early Erastothian aged crater.

However, the rock abundance anomaly is inconsistent with either of the surface rock production and preservation models described above. First, the rock abundances are much higher than other massive impact melt deposits, including younger deposits such as those found at Theophilus and larger deposits such as those found SW of Orientale Basin (Williams et al., this issue). Second, given the roughly symmetric distribution of thick non-rocky ejecta and impact melt deposits about the crater (green and red units in Fig. 2F), the emplacement of large block-rich ejecta and

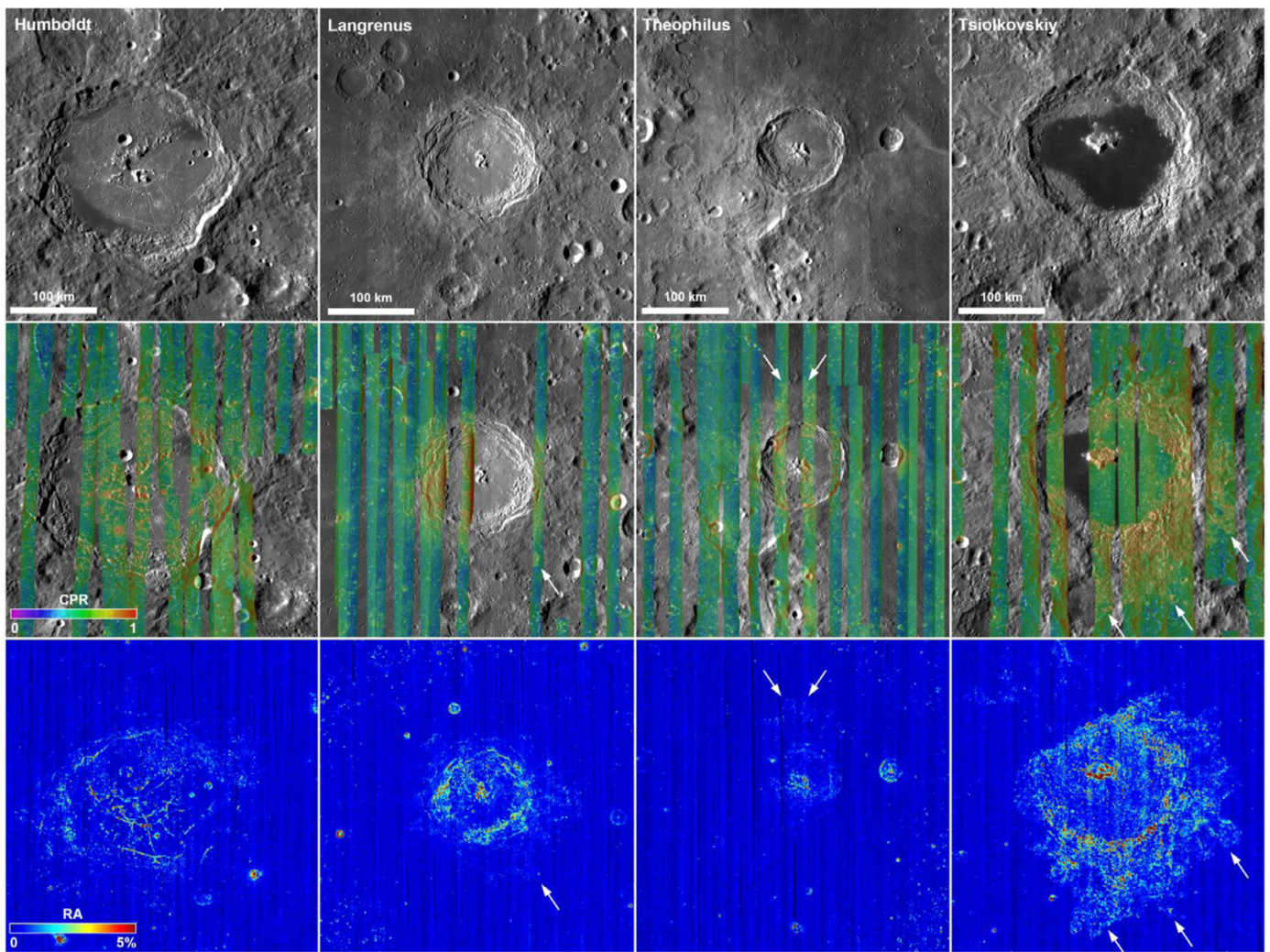


Fig. 7. A comparison of craters Humboldt, Langrenus, Theophilus, and Tsiolkovskiy (left-to-right). For each crater, LROC morphological maps, Mini-RF CPR overlaid on same-sense radar, and Diviner rock abundance data are shown at the same scale. Tsiolkovskiy has significantly better preserved impact melt and higher rock abundances across a larger area than the other craters (arrows).

subsequent degradation should be more symmetric. Provided the spatial correlation between the rock abundance anomaly and the massive impact melt deposit, we propose a third, hybrid model (Fig. 9E and F). In this model, large blocks from ejecta are entrained in massive impact melt that forms an extensive melt flow, likely with large plates and rafts. Given the consolidated nature of this deposit, any small impactor that can penetrate the regolith will produce surface rocks either from direct ejection or seismically-induced regolith removal from the tops of nearby large blocks (also the basis for the hummocky terrain). Relative to the standalone impact melt and primary ejecta rock production models, this hybrid model produces more surface rocks and results in a thinner regolith cover for a given age. This massive impact melt and large block-rich ejecta deposit would have morphological similarities to the non-mare crater floor, which is characterized by megablocks entrained in a massive coherent impact melt pond. As described in Sections 3.2 and 3.3, the surface rock populations within these units at Tsiolkovskiy do share similar morphologies and spatial distributions. However, this hybrid mechanism would need to be unique in order to fully explain the relative magnitude or spatial extent of the Tsiolkovskiy rock abundance anomaly, which is unlikely given the prevalence of both impact melt and primary ejecta on the Moon.

4.3. Reconciling high rock abundances in an ancient crater

Tsiolkovskiy has substantial evidence for an ancient origin and yet has surface rock abundances consistent with much younger features. Using relative stratigraphy and a variety of crater-counting methods, Tsiolkovskiy has been consistently dated to the Late Imbrian period (Gornitz, 1973; Wilhelms and El-Baz, 1977; Walker and El-Baz, 1982; Wilhelms, 1987; Tyrie, 1988); however, recent crater-counting studies using high resolution imagery from LROC have suggested a lower-limit age for Tsiolkovskiy closer to the Imbrian–Erastothenean boundary around 3.2 Ga, based on the age of mare and ejecta deposits (Pasckert et al., 2015, this study). Applying the rock abundance chronology of Ghent et al. (2014) to all parts of the crater including impact melt, we find that Tsiolkovskiy's rock abundance anomaly has a block population similar to Copernican craters, and its H -parameter values (Hayne et al., this issue) indicate the average rock-free regolith thickness is consistent with <1.5 Ga of surface exposure. Here we discuss three scenarios that could explain these observations.

First, Tsiolkovskiy may have produced an anomalously large volume of impact melt and ejected more, larger blocks compared to its contemporary crater population. Large craters are capable

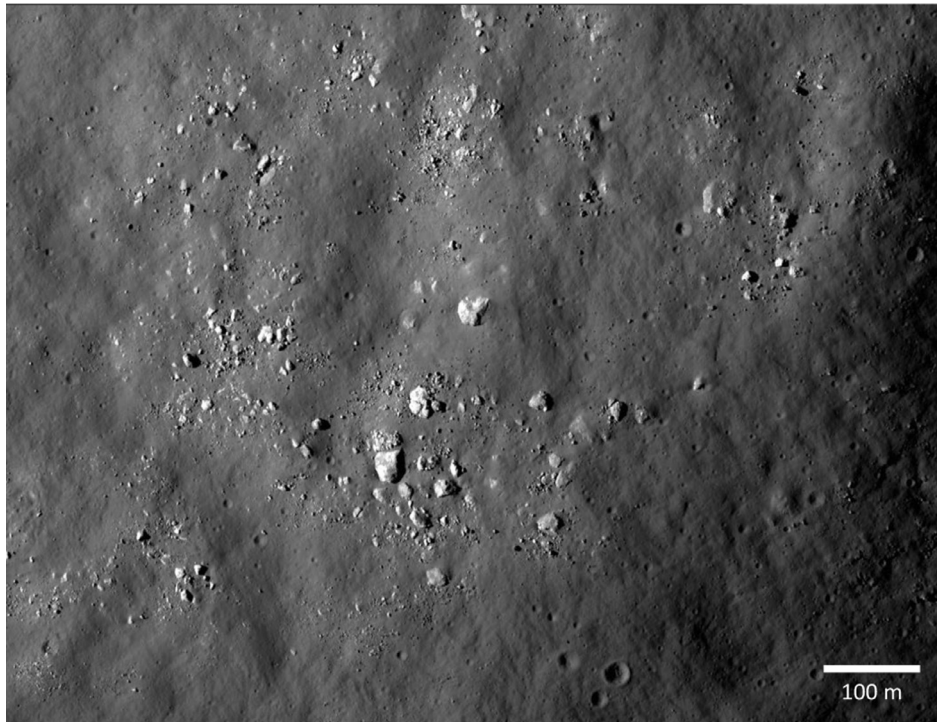


Fig. 8. Boulders and large blocks are found throughout the rock abundance anomaly. In this image blocks as large as 50m in diameter are shown with various degrees of regolith cover ranging from nearly buried to well exposed above the local terrain (21.14°S/132.81°E). The image resolution is ~ 1.2 m/pixel with 73.3° solar incidence (LROC NAC Frame: M149648914L).

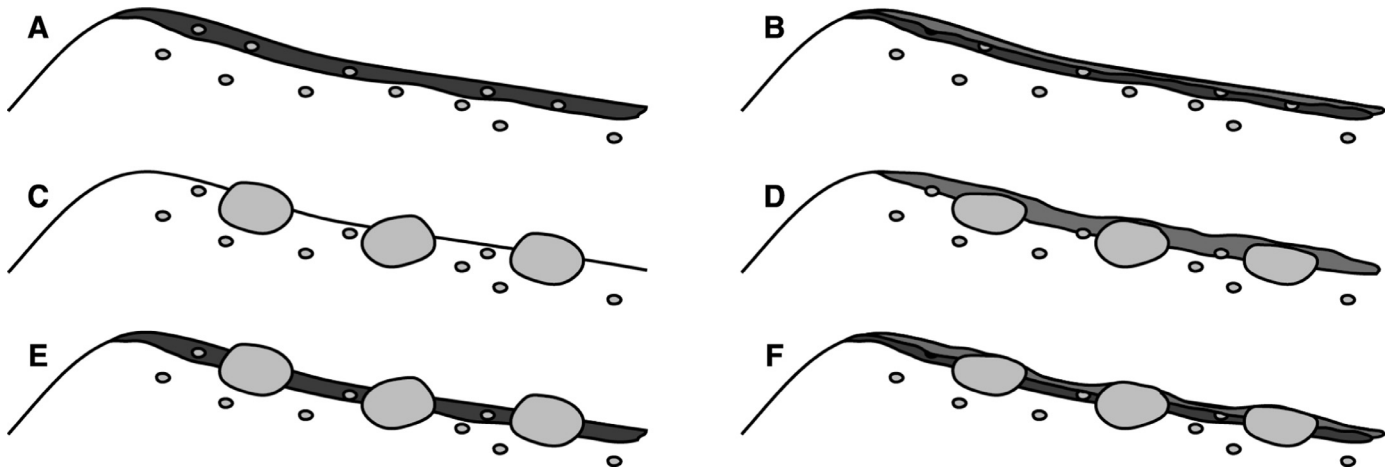


Fig. 9. This simple (not-to-scale) illustration depicts the role of impact melt (dark gray) in preserving primary ejecta rich in boulders and large blocks (white and light gray). Typical fresh impact melt (A) is relatively smooth, cohesive flow with few entrained boulders. After ~ 1 Ga of exposure (B), a thin, uniform regolith (medium gray) has developed. New surface rocks are only produced from impacts large enough to penetrate the regolith and reach the buried impact melt. Impact ejecta rich in boulders and large blocks (C) will initially have abundant surface and subsurface rocks. However, after ~ 1 Ga of exposure (D), surface rocks are broken down and a thick layer of gardened regolith has developed. New surface rocks are only produced from impacts into sparsely-distributed, buried large blocks. Emplaced impact melt rich with entrained boulders and large blocks (E) initially forms an extensive cohesive, rough flow. After ~ 1 Ga of exposure (F), regolith is relatively thin, but less uniform than (B). New surface rocks are produced from impacts into both buried impact melt and large blocks, and impact-induced shaking thins and or removes regolith from large blocks.

of producing larger amounts of impact melt by volume (Melosh, 2011) and are more capable of ejecting large blocks. Given its 180 km size and apparent age near the Imbrian–Erastothenean boundary, Tsiolkovskiy may be the largest crater of its age and therefore represents the last impact event capable of producing such a deposit. However, Tsiolkovskiy is only modestly larger than Hausen crater (65.5°S, 88.4°W; ~ 167 km diameter Erastothenean crater; Wilhelms, 1987), which displays a typical block population. Still, target properties, such as pre-impact terrain, and oblique impact geometry (Hawke and Head, 1977; Craddock and Greeley, 1988) may have been unusually favorable for melt formation

and preservation. Although vertical impact will produce more impact melt than oblique impacts (Plescia and Cintala, 2012), the Tsiolkovskiy-forming impact may have resulted in unusual spatial distribution of impact melt and a thicker deposit. In this scenario, the rock abundance anomaly is derived predominantly from the original massive impact melt and large block-rich ejecta deposit via subsequent (presumably typical) local impacts and regolith gardening.

Second, Tsiolkovskiy may have experienced a large regolith removal event during the Copernican Period caused by an antipodal or regional event. The antipode of Aristarchus crater is located

just off the southeast rim of Tsiolkovskiy (Fig. 2A – orange circle) and is near the region of highest rock abundances (Fig. 2B). However, Tsiolkovskiy's rock abundance anomaly deposit is widespread (~200 km) compared to the relatively small Aristarchus-forming impact (~40 km diameter crater). For comparison, there is also a rock abundance anomaly at the antipode of Tycho crater, a much larger impact, that is limited to approximately the diameter of Tycho (~80 to 100 km) (Bandfield et al., 2011). Furthermore, we do not find evidence for the Diviner spectral signature for the high silica materials Glotch et al. (2010) found in Aristarchus crater and local ejecta that would implicate antipodal ejecta deposits. However, even without evidence for ejecta produced surface rocks, the regolith removal process may involve shaking from impacts combined with stripping or sloughing off of regolith fines. More regionally, Tsiolkovskiy lies at the end of a bright ray (Fig. 1) and a soil temperature anomaly starting at Giordano Bruno and passing through King and Necho craters. Any of these events could have affected the area near Tsiolkovskiy; however, the magnitude of these events is currently poorly understood and would benefit from additional seismic modeling. In this scenario, Tsiolkovskiy's rock abundance anomaly is derived from more typical impact melt and ejecta block populations from the original impact event that has been recently uncovered by large-scale seismic-shaking from a regional or antipodal impact event.

Finally, and perhaps most plausibly, these scenarios can be combined to decrease the dependence on extreme conditions or events. The rock abundance anomaly observed at Tsiolkovskiy is clearly associated with a massive impact melt deposit observed by Mini-RF and large blocks clearly play a role in the evolution of the rock abundance anomaly. Regolith removal events must be relatively common; however, this rock abundance anomaly is unique. Therefore, in this scenario, we invoke an unusually massive impact melt deposit that includes large blocks, combined with unusually thin regolith cover that promotes the formation of surface rocks, likely caused by a surface modification event in the last ~1 Ga.

5. Conclusions

In this study, we analyzed the rock population and distribution around Tsiolkovskiy crater. This study was enabled by new datasets from LRO that provide information on the surface and near-subsurface rock populations at a variety of spatial scales and wavelengths. We found that Tsiolkovskiy has an external deposit where (1) Diviner rock abundance is anomalously high, similar to Copernican-aged craters, (2) Diviner estimates of rock-free regolith thickness are anomalously low, consistent with <1.5 Ga of regolith gardening, (3) Mini-RF CPR indicates well preserved massive impact melt, which is rough at the decimeter-scale, and (4) LROC imagery provides clear examples of surface rock population morphology similar to the crater interior. Furthermore, we used LROC imagery to perform a new calculation of absolute modeled crater age consistent with an ancient origin (at least 3.2 Ga). Together these data show that Tsiolkovskiy has a uniquely well-preserved massive impact melt and blocky ejecta deposit for a crater of its size and age, and may be the youngest lunar crater capable of producing this type and scale of deposit.

To reconcile the anomalously rocky appearance of Tsiolkovskiy with its age we proposed mechanisms that support a higher surface rock production rate invoking (1) Tsiolkovskiy's size, target properties, and/or impact geometry to produce a massive impact melt deposit with sufficient large blocks, and (2) the recent disruption of surface fines exposing original blocks from local, regional, and/or antipodal impacts. The source of this disruption is unknown, but Tsiolkovskiy crater is located antipodal to the Copernican-aged Aristarchus crater. Future modeling of the seismic effects of this impact may help to determine whether this was

a likely source for the recent surface modification at Tsiolkovskiy crater.

Acknowledgments

We thank the LRO, Diviner, Mini-RF, and LROC operations teams for their effort in returning the data presented here. We also wish to thank the Diviner and Mini-RF science teams for helpful discussion in the early stages of this work. This work was supported by the LRO project and the Diviner science investigation, under contract with NASA.

References

- Bandfield, J.L., Ghent, R.R., Vasavada, A.R., et al., 2011. Lunar surface rock abundance and regolith fines temperatures derived from LRO Diviner Radiometer data. *J. Geophys. Res.* 116, E00H02. doi:10.1029/2011JE003866.
- Barabashov, N.P., 1962. Structure of the Moon's surface and investigation of the first photographs of its far side. *Int. Geol. Rev.* 4 (6), 631–634.
- Basilevsky, A.T., Head, J.W., 2012. Age of Giordano Bruno crater as deduced from the morphology of its secondaries at the Luna 24 landing site. *Planet. Space Sci.* 73, 302–309.
- Boyce, J.M., Johnson, D., 1977. Ages of flow units in Mare Crisium based on crater density. In: *Proceeding of the 8th Lunar and Planetary Science Conference*, pp. 3495–3502.
- Cahill, J.T.S., Thomson, B.J., Patterson, G.W., et al., 2014. The Miniature Radio Frequency instrument's (Mini-RF) global observations of Earth's Moon. *Icarus* 243, 173–190.
- Campbell, B.A., 2002. *Radar Remote Sensing of Planetary Surfaces*. Cambridge University Press, Cambridge, U.K.
- Carter, L.M., Neish, C.D., Bussey, D.B.J., et al., 2012. Initial observations of lunar impact melts and ejecta flows with the Mini-RF radar. *J. Geophys. Res.* 117, E00H09. doi:10.1029/2011JE003911.
- Cheek, L.C., Pieters, C.M., 2012. Variations in anorthosite purity at Tsiolkovsky crater on the Moon. In: *Proceeding of the 43rd Lunar and Planetary Science Conference*.
- Craddock, R., Greeley, R., 1988. Thickness and volume of mare deposits in Tsiolkovsky, lunar farside. In: *Proceeding of the 18th Lunar and Planetary Science Conference*, pp. 331–337.
- Ghent, R.R., Hayne, P.O., Bandfield, J.L., et al., 2014. Constraints on the recent rate of lunar ejecta breakdown and implications for crater ages. *Geology* 42 (12), 1059–1062.
- Ghent R.R., Carter L.M., Bandfield J.L., Tai Udovicic C.J., Campbell B.A., Lunar crater ejecta: Physical properties revealed by radar and thermal infrared observations, *Icarus*, In Press, Corrected Proof, Available online 24 December 2015.
- Glotch, T.D., Lucey, P.G., Bandfield, J.L., et al., 2010. Highly silicic compositions on the Moon. *Science* 329 (5998), 1510–1513. doi:10.1126/science.1192148.
- Gornitz, V., 1973. Igneous vs impact processes for the origin of the mare lavas. *Moon* 6, 357–379.
- Greenhagen, B.T., Neish, C.D., Bandfield, J.L., et al., 2013. Anomalously fresh appearance of Tsiolkovsky crater: Constraints from Diviner, Mini-RF, and LROC. In: *Proceeding of the 43rd Lunar and Planetary Science Conference*.
- Guest, J.E., Murray, J.B., 1969. Nature and origin of Tsiolkovsky crater, lunar farside. *Planet. Space Sci.* 17, 121–141.
- Guest, J.E., 1971. *Geology and Physics of the Moon; A Study of Some Fundamental Problems*. Elsevier, London, pp. 93–104.
- Hawke, B.R., Head, J.W., 1977. Impact melt on lunar crater rims. *Impact and Explosion Cratering*. Pergamon Press, New York, NY, pp. 815–841.
- Hayne, P.O. et al., (2015) this issue.
- Howard, K.A., Wilshire, H.G., 1975. Flows of impact melt at lunar craters. *J. Res. US Geol. Surv.* 3, 237–251.
- Matsunaga, T., Ohtake, M., Haruyama, J., et al., 2008. Discoveries on the lithology of lunar crater central peaks by SELENE spectral profiler. *Geophys. Res. Lett.* 35, L23201. doi:10.1029/2008GL035868.
- Melosh, H.J., 2011. *Planetary Surface Processes*. Cambridge University Press, Cambridge, U.K.
- Michael, G.G., Neukum, G., 2010. Planetary surface dating from crater size-frequency distribution measurements: Partial resurfacing events and statistical age uncertainty. *Earth Planet. Sci. Lett.* 294 (3–4), 223–229.
- Morota, T., Haruyama, J., Miyamoto, H., et al., 2009. Formation age of the lunar crater Giordano Bruno. *Meteorit. Planet. Sci.* 44, 1115–1120. doi:10.1111/j.1945-5100.2009.tb01211.x.
- Neish, C.D., Bussey, D.B.J., Spudis, P., et al., 2011. The nature of lunar volatiles as revealed by Mini-RF observations of the LCROSS impact site. *J. Geophys. Res.* 116 (E1). doi:10.1029/2010JE003647.
- Neish, C.D., Greenhagen, B.T., Patterson, G.W., et al., 2013. Impact melt deposits at Tsiolkovskiy crater: Constraints on crater age. In: *Proceeding of the 43rd Lunar and Planetary Science Conference*.
- Neish, C.D., Madden, J., Carter, L.M., et al., 2014. Global distribution of lunar impact melt flows. *Icarus* 239, 105–117.
- Neukum, G., Ivanov, B.A., Hartmann, W.K., 2001. Cratering records in the inner Solar System in relation to the lunar reference system. *Space Sci. Rev.* 96, 55–86.

- Nozette, S., Spudis, P., Bussey, B., et al., 2010. The Lunar Reconnaissance Orbiter Miniature Radio Frequency (Mini-RF) technology demonstration. *Space Sci. Rev.* 150, 285–302.
- Paige, D.A., Foote, M.C., Greenhagen, B.T., et al., 2010. The Lunar Reconnaissance Orbiter Diviner lunar radiometer experiment. *Space Sci. Rev.* 150, 125–160.
- Pasckert, J.H., Hiesinger, H., van der Bogert, C.H., 2015. Small-scale lunar farside volcanism. *Icarus* 257, 336–354.
- Plescia, J.B., Cintala, M.J., 2012. Impact melt in small lunar highland craters. *J. Geophys. Res.* 117, E00H12. doi:10.1029/2011JE003941.
- Pieters, C.M., Tompkins, S., 1999. Tsiolkovsky crater: A window into crustal processes on the lunar farside. *J. Geophys. Res.* 104 (E9), 21935–21949.
- Robinson, M.S., Brylow, S.M., Tschimmel, M., et al., 2010. Lunar Reconnaissance Orbiter Camera (LROC) instrument overview. *Space Sci. Rev.* 150, 81–124.
- Shankar, B., Osinski, G.R., Antonenko, I., et al., 2013. A multispectral geological study of the Schrödinger impact basin. *Can. J. Earth Sci.* 50 (1), 44–63. doi:10.1139/e2012-053.
- Tyrie, A., 1988. Age dating of mare in the lunar crater Tsiolkovsky by crater-counting method. *Earth Moon Planets* 42, 245–264.
- Walker, A.S., El-Baz, F., 1982. Analysis of crater distributions in mare units on the lunar far side. *Moon Planets* 27 (1), 91–106.
- Whitford-Stark, J.L., Hawke, B.R., 1982. Geologic studies of the lunar far side crater Tsiolkovsky. In: *Proceeding of the 13th Lunar and Planetary Science Conference*.
- Wilhelms, D., 1987. The geologic history of the Moon. USGS Professional Paper, 1348. USGS.
- Wilhelms, D.E., El-Baz, F., 1977. Geologic map of the east side of the Moon. USGS Miscellaneous Investigations Series, Map I-948. USGS.
- Williams, J.-P., Petro, N.E., Greenhagen, B., et al., 2013. Inferred age of mare fill in Tsiolkovskiy crater: Constraints on the preservation of exterior impact melt deposits. In: *Proceeding of the 43rd Lunar and Planetary Science Conference*.
- Williams, J.-P. et al., (2015) this issue.